Article

Mimicking Multiorbital Systems with SU(*N*) Atoms: Hund's Physics and Beyond

Andrea Richaud [1],*, Matteo Ferraretto [1] and Massimo Capone [1,2]

1   Scuola Internazionale Superiore di Studi Avanzati (SISSA), Via Bonomea 265, I-34136 Trieste, Italy; mferrare@sissa.it (M.F.); capone@sissa.it (M.C.)
2   CNR-IOM Democritos, Istituto Officina dei Materiali, Consiglio Nazionale delle Ricerche, Via Bonomea 265, I-34136 Trieste, Italy
*   Correspondence: arichaud@sissa.it

Abstract: The physics of many interesting correlated materials can be captured by multiorbital Hubbard models, where conduction electrons feature an additional orbital degree of freedom. The multiorbital characteristic is not a mere complication, but it leads to an immensely richer landscape of physical regimes. One of the key features is the interplay between Hubbard repulsion and Hund's exchange coupling, which has been shown to lead to orbital-selective correlations and to the existence of correlation-resilient metals (usually called Hund's metals) defying Mott localization. Here, we show that experimentally available platforms of SU(*N*)-symmetric ultracold atoms can indeed mimic the rich physics disclosed by multiorbital materials, by exploiting the internal degrees of freedom of multicomponent atoms. We discuss in detail the SU(*N*) version of interaction-resilient Hund's metal and some other interesting regimes.

Keywords: SU(*N*) atoms; multicomponent systems; Mott transition; Hund's metals

1. Introduction

A large number of materials with conceptual and practical interest require a multiorbital description, in which different atomic levels must be taken into account. When we focus on strongly correlated materials, this means that the interaction is not given purely by the Hubbard interaction U, but it also contains an exchange coupling J, called Hund's coupling (see Appendix A). The interplay between these two terms is the key that opens the path to a wide range of new states and physical regimes. In this manuscript, we take a broader perspective and we show that similar physics can be realized in a wider class of multicomponent quantum systems when the Hubbard U competes with other energy scales.

In the case of solid-state multiorbital models, the U-term penalizes spatial charge fluctuations (local occupancies different from the average filling), while the J-term favors high-spin configurations and, to a lesser degree, high orbital angular momentum [1–3]. This competition results in an extremely rich scenario of intriguing quantum phases, such as orbital-selective Mott phases (where some bands undergo Mott localization, while others remain metallic) [4–7], orbital-selective superconductors [8] and the so-called "Hund's metal" [2,9–12]. These regimes, besides their conceptual interest, have been invoked to understand the properties of different materials, among which iron-based superconductors [13,14] and ruthenates [15]. In particular, "Hund's metal" characterizes the phase diagram of $N-$orbital Hubbard models at integer filling different from N, when U and J are such that $J/U \approx 1/3$. This state is rather surprising, since it retains metallic properties in spite of very large values of U and J, two terms which, individually, would constrain electron mobility. The mechanism which supports the existence of these interaction-resilient metals was understood to be the competition between two strongly correlated insula-

tors [9], namely, a high-spin Mott insulator stabilized by large values of U and a charge-disproportionated insulator [16], dubbed "Hund's insulator", favored by J.

While the direct quantum simulation of a multiorbital Hubbard model with Hund's coupling performed by means of cold atomic systems is an extremely hard task, as one should introduce both an orbital and a spin degree of freedom, SU(N)-interaction-symmetric Hubbard models can be effectively simulated by means of ultracold ^{87}Sr [17], ^{173}Yb [18] and ^{6}Li atoms [19,20] loaded in optical lattices [21–29]. Thanks to their peculiar atomic structure (see Section 2), they offer up to ten nuclear-spin flavors which cannot undergo recombinations upon scattering events.

In this paper, we show that the interesting physics occurring in multiorbital solid-state systems can be effectively mimicked by experimentally available multiflavor atomic platforms. We substantiate this claim by thoroughly investigating the properties of an SU(3) Hubbard model with a suitable single-particle patterned potential, whose phase diagram hosts different kinds of strongly correlated insulators, as well as interaction-resilient metallic regions. We discuss how this scenario mirrors the one disclosed by the three-orbital Hubbard–Kanamori model with two particles per site (filling factor $\langle n_i \rangle = 2$). Furthermore, we argue that the mechanism supporting the existence of persistently metallic solutions in the atomic platform is identical to the one underlying the emergence of Hund's metals.

This manuscript is organized as follows: In Section 2, we present the SU(N) Hubbard model and discuss its basic properties. In Section 3, we discuss how SU(N) ultracold platforms can be used to mimic the emergence of Hund's metals. Section 4 is devoted to future perspectives on the quantum simulation of multiorbital materials, as well as to concluding remarks.

2. The SU(N) Hubbard Model: Basic Properties and Some Extensions

The SU(N) generalization of the well-known Hubbard model is usually written as

$$H = -t \sum_{\langle i,j \rangle} \sum_{m=1}^{N} \left(c_{i,m}^{\dagger} c_{j,m} + \text{h.c.} \right) + \frac{U}{2} \sum_{i} n_i(n_i - 1) \tag{1}$$

where the operator $c_{i,m}$ annihilates a fermion with flavor m at lattice site i, $n_i := \sum_m n_{i,m} := \sum_m c_{i,m}^{\dagger} c_{i,m}$ is the total number operator at site i and the summation $\sum_{\langle i,j \rangle}$ runs over nearest-neighbor lattice sites [30]. This Hamiltonian appropriately captures the low-energy physics of alkaline-earth or alkaline-earth-like atoms, whose unique atomic structure (namely, highly decoupled nuclear and electronic spin degrees of freedom) results in SU(N)-invariant interatomic interactions, since flavor redistribution upon scattering events is inhibited [21–29]. As an example, ^{87}Sr [17], ^{173}Yb [18] and ^{6}Li atoms [19,20] have nuclear spin $I = 9/2$, $I = 5/2$ and $I = 1$, respectively; thus, they offer up to ten, six, or three different nuclear spin states, respectively (henceforth called flavors), although it is common to select a subset of flavors $\{m\}$ out of the $N = 2I + 1$ available [31].

The rich physical scenario exhibited by Hamiltonian (1) originates from the competition between hopping processes $\propto t$ and interactions $\propto U$. Usually, in experimental setups, the ratio t/U can be tuned by varying the depth of the optical lattice, while temperature T can be lowered down to $< t/k_B$ [30]. Regarding the ground state of Hamiltonian (1), when $t \gg U$ (or away from integer fillings), the system is typically metallic. Conversely, for integer fillings $n = 1, 2, \ldots, N$ and in presence of strong interactions $U \gg t$, a Mott-insulating state can be stabilized. The latter is distinguished by a strong suppression of spatial charge fluctuations, which would involve an energy cost $\approx U$ [18].

Hamiltonian (1) can be supplemented by additional processes [32], either in order to better model a real-world experimental apparatus (e.g., to account for the presence of an external, often harmonic, trapping potential), or to access even wider and more interesting physical scenarios, such as the quantum simulation of multicomponent materials. It is in this spirit that an optical superlattice, i.e., an extra site-dependent single-particle potential, is introduced in Section 3. The ensuing model has been shown to effectively mimic the physics of Hund's metals in an experimentally accessible ultracold atomic platform [9,11].

In the same spirit, Raman scattering processes can be introduced by means of suitable laser beams, in order to allow flavors to be redistributed, hence explicitly breaking the SU(N) symmetry of the system. These processes can be effectively described by introducing an extra inter-flavor, intra-site tunneling term in Hamiltonian (1). As demonstrated in a recent study by Tusi et al. [33], the resulting model gives access to the atomic counterpart of the well-known orbital-selective Mott transition [4,5] occurring in multiorbital solid-state systems.

3. Mimicking Hund's Physics via SU(N) Ultracold Atoms

In solid-state physics, the multiorbital Hubbard–Kanamori model is known to describe the strongly correlated Hund's metal, i.e., a state that is persistently metallic in spite of strong interactions and integer fillings [2]. This class of interaction-resilient metals can be regarded as a bridge between two strongly correlated insulators, a high-spin Mott insulator and a charge-disproportionated insulator, which goes under the name of Hund's insulator (see Ref. [9] for a thorough analysis based on rotation-invariant slave bosons and Appendix A for a pedagogical introduction based on the exact diagonalization of a three-site system). In essence, Hund's metal constitutes the compromise between two competing insulators and its metallic character is supported by the forced coexistence of their typical atomic multiplets.

In Ref. [11], we showed that Hund's metal is just a specific realization of a more general phenomenon, which can be present in various strongly correlated systems. In particular, we showed that an SU(3) Hubbard model with patterned single-particle potential can be engineered in such a way to trigger the emergence of interaction-resilient metallicity. The Hamiltonian of the model reads

$$H = -t \sum_{j=1}^{L} \sum_{m=1}^{3} \left(c_{j,m}^{\dagger} c_{j+1,m} + \text{h.c.} \right) + \frac{U}{2} \sum_{j=1}^{L} n_j (n_j - 1) + \sum_{j=1}^{L} \mu_j n_j, \tag{2}$$

which constitutes the one-dimensional three-flavor version of Hamiltonian (1), with the additional presence of a superlattice of the form

$$\mu_j = \begin{cases} -\mu, & \text{if } j \bmod 3 = 1 \\ 0, & \text{if } j \bmod 3 = 2 \\ -\mu, & \text{if } j \bmod 3 = 0 \end{cases} \tag{3}$$

with $\mu > 0$. At global average filling $\langle n_i \rangle = 2$, the peculiar pattern of this single-particle potential favors a charge-ordered state, where lower-energy sites are completely filled and higher-energy sites are completely empty (see the bottom panel of Figure 1 for a pictorial representation). In opposition to the tendency of occupying low-energy sites, the Coulomb interaction U penalizes charge fluctuations in the form of local occupancies different from $\langle n_i \rangle = 2$ (see the top panel of Figure 1). This model and the physics which it discloses are within the reach of current experimental apparatuses; multicomponent [87]Sr [17], [173]Yb [18] and [6]Li [19,20] fermionic quantum gases can be conveniently prepared in such a way to realize a balanced mixture of only $N = 3$ flavors, which can then be loaded into a suitable optical lattice [21]. In order to realize the single-particle potential of Equation (3), i.e., a lattice with a three-site unit cell, the atomic gas must be loaded into a suitable superposition of optical lattices of different spatial periods, such that the resulting laser intensity reflects the desired pattern. In one dimension [31], for example, one can interfere laser beams in such a way to make the energy of one site out of three higher than that of the other sites [34,35]. Similarly, in two dimensions [36], one can conveniently design triangular [37] or Kagome lattices [38] whose inherently triangular geometry naturally mirrors the three-site structure of the aforementioned unit cell.
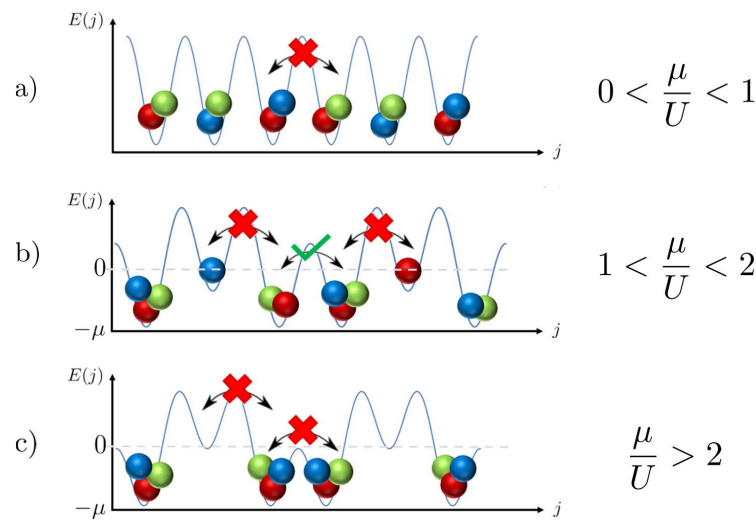
Figure 1. Schematic illustration of the three different classes of insulators. Panel (**a**): Mott insulator. Panel (**b**): intermediate phase. Panel (**c**): Band insulator. In all panels, the elementary unit cell of three sites is repeated twice. In panel (**a**), we drew the potential setting $\mu \to 0$.

It is worth mentioning that Hamiltonian (2) can also be regarded as the three-flavor three-site-unit-cell version of the ionic Hubbard model [39–47], where a standard Mott insulator competes with a charge-density-wave insulator. In the associated phase diagram, these two insulating solutions are known to be separated by a narrow stripe-like region, where, depending on the system dimensionality, a metallic [48] or a bond-order-wave phase [49] (featuring staggered kinetic energy on the bonds) can be found.

3.1. Competing Correlated Insulators

As the competition between the Coulomb repulsion U and Hund's exchange coupling J results in the emergence of Hund's metals (see Appendix A) in multiorbital materials, so, in our SU(3)-symmetric atomic platform, the competition between U and the single-particle patterned potential μ results in persistently metallic solutions. To illustrate the occurrence of this phenomenon, we showed that it is possible to focus on a minimal cluster of three sites [11], which can be regarded as the elementary building block of larger and higher-dimensional lattices, as well as of more sophisticated quantum cluster theories [50–53]. This choice allowed us to capture the essential physics of the problem and, in parallel, to develop simple analytical arguments and the exact numerical diagonalization of the associated Hamiltonian. In the atomic limit ($t = 0$), one can easily recognize the presence of three distinct regimes for the ground state, as follows:

1. For $0 < \mu/U < 1$, the system is a Mott insulator (see top panel of Figure 1), whose energy is $E_{MI} = 3U - 4\mu$. Due to the strong interaction U and weak on-site potential μ, spatial charge fluctuations are forbidden and exactly two fermions occupy each site.
2. For $1 < \mu/U < 2$, there are two degenerate ground states, such that the high-energy site hosts one fermion, while the low-energy sites host either two or three fermions (see central panel of Figure 1). The associated energy reads $E_{INT} = 4U - 5\mu$.
3. For $\mu/U > 2$, the large on-site potential μ wins the Hubbard repulsion U and the system is a charge-disproportionated insulator, where the low-energy sites are completely filled, while the high-energy site is empty (see bottom panel of Figure 1). This configuration, whose energy is $E_{BI} = 6U - 6\mu$, constitutes the atomic version of a band insulator.

We remark that the aforementioned MI state and the BI state respectively mirror the high-spin Mott insulator and the Hund's insulator solutions that characterize the phase diagram of the three-orbital Hubbard–Kanamori model (see Appendix A). As opposed to the latter model, where the two different insulators are degenerate only along a specific

line ($J/U = 1/3$) of the phase diagram, Hamiltonian (2) admits an intermediate solution for $1 < \mu/U < 2$, where hopping is possible only between pairs of neighboring low-energy sites (while high-energy sites constitute insulating barriers). Such a phase intercalates between the MI and the BI solutions, to which it is degenerate along the lines $\mu/U = 1$ and $\mu/U = 2$, respectively, since one can verify immediately that $E_{MI} = E_{INT}$ along the line $\mu/U = 1$ and that $E_{BI} = E_{INT}$ along the line $\mu/U = 2$.

3.2. Interaction-Resilient Metallicity

Moving away from the atomic-limit analysis discussed in the previous section, we analyze the conduction properties of the ground state of Hamiltonian (2) by means of exact numerical diagonalization. To perform this, we consider the simplest possible closed circuit, namely, a three-site system with periodic boundary conditions (a ring trimer). In spite of its very few sites, this system has been shown to be an effective minimal lattice in the investigation of a number of physical phenomena, for both fermionic [54–57] and bosonic [58–65] systems. We compute the current flowing therein upon rotating the system around its axis, in such a way that, working in the rotating frame of reference, the Coriolis force can induce a particle current in the ring [66–69]. We recall that the effect of the Coriolis force is formally equivalent to the effect of a magnetic flux Φ threading the ring in the case of electrically charged particles [70]. As a consequence, one can simply implement the rotation by performing the Peierls substitution, i.e., replacing the hopping term in Hamiltonian (2) with

$$H_{\text{hop}} = -t \sum_{j=1}^{L} \sum_{m=1}^{3} \left(e^{i\frac{\Phi}{L}} c_{j,m}^{\dagger} c_{j+1,m} + \text{h.c.} \right), \tag{4}$$

where the Peierls phase Φ is proportional to the Coriolis force. Notice that the interaction term $\propto U$, as well as the single-particle-potential term $\propto \mu$ are left unchanged by the Peierls substitution. The ground state $|\psi_0'\rangle$ of the resulting Hamiltonian, H', is characterized in terms of the expectation value of the particle current operator [71,72]

$$I = \langle \psi_0' | -\frac{\partial H'}{\partial \Phi} | \psi_0' \rangle, \tag{5}$$

whose magnitude mirrors the degree of metallicity of the system [73]. More specifically, in the context of electrically charged particles, if the applied magnetic flux is small, the current I is proportional to the "Drude weight" [68], a quantity which is, in turn, proportional to the singular part of the DC electrical conductivity. One can thus take advantage of observable (5) to reconstruct a conductivity-based phase diagram.

The results, reported in Figure 2, confirm the scenario presented in Section 3.1 and pictorially illustrated in Figure 1; at strong coupling ($U/t \gg 1$) and small values of μ/t, the system is a Mott-insulator and the current is suppressed because of the Coulomb repulsion which penalizes triple occupancies. On the other hand, when the single-particle patterned potential μ/t is large and U/t is small, the system is a band insulator and particle hoppings are suppressed not to pay the energy cost of populating high-energy sites. In addition to the two aforementioned kinds of insulating solutions, one can recognize a third insulating region between the lines $\mu/U = 1$ and $\mu/U = 2$, where the overall conduction is suppressed because charge fluctuations on the high-energy site are quenched.

Interestingly, one can appreciate the presence of two distinct regions where the current is remarkably large in spite of the strong Coulomb repulsion and of the deep superlattice. They are two stripes centered about the lines $\mu/U = 1$ and $\mu/U = 2$, which represent the two degeneracy conditions for the three solutions of the atomic limit, i.e., $E_{MI} = E_{INT}$ and $E_{INT} = E_{BI}$, respectively (see Section 3.1). In analogy with the physics of multiorbital correlated materials [9,11] (see also Appendix A), we find that the competition between two different correlated insulators gives place to a persistently metallic solution.
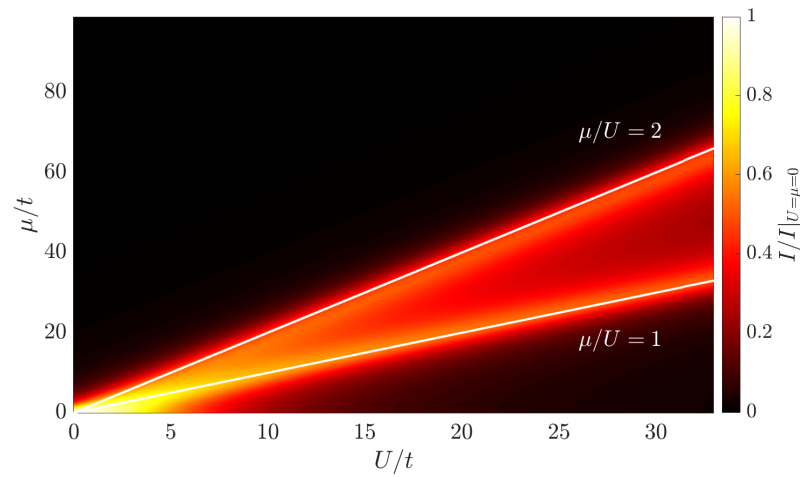
Figure 2. Expectation value of the current operator (see Equation (5)) as a function of U/t and μ/t, for a system of $L = 3$ sites, global filling $\langle n_i \rangle = 2$ and flux $\Phi = 0.4\pi$. Black (white) regions correspond to insulating (highly conductive) states.

3.3. The Key Role of Local Configurations

The presence of interaction-resilient metallicity can be understood in terms of populations of different local configurations, i.e., $p_n(j) = \sum |\langle n_j | \psi_0 \rangle|^2$, where $|\psi_0\rangle$ is the ground state of Hamiltonian (2) and $|n_j\rangle$ are states with exactly n fermions at site j. In essence, the competition between μ and U creates situations where neighboring sites host a fluctuating number of particles, which, being compatible with hopping processes of the type $c^\dagger_{j,m} c_{j\pm 1,m}$, can support current flow, hence the metallic properties of the system.

The functional dependence of $\bar{p}_n = (1/3) \sum_{j=1}^{3} p_n(j)$, i.e., the weight of the four possible local configurations mediated over all the three lattice sites, on the control parameter μ/U is illustrated in Figure 3. In the strongly interacting regime and for $\mu/U \ll 1$, all sites essentially host exactly $n = 2$ fermions because the system is in a Mott-insulating state (see top panel of Figure 1). Conversely, for $\mu/U \gg 2$, the system is in a band-insulating state (see bottom panel of Figure 1), a regime where one-third of the sites are empty ($n = 0$) and two-thirds of the sites are filled by $n = 3$ fermions. Similarly, in the intermediate phase, for example at $\mu/U = 1.5$, the weights of local configurations with $n = 1, 2, 3$ are similar and approximately equal to $1/3$.
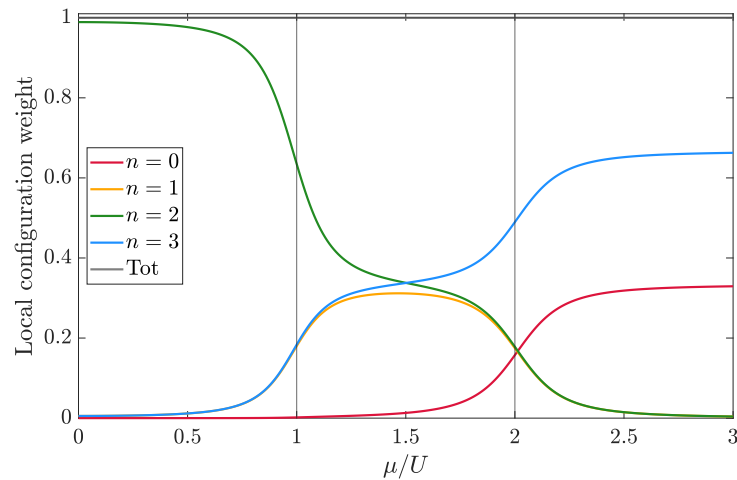

Figure 3. Population of single-site states as a function of μ/U. Results from the exact numerical diagonalization of Hamiltonian (2) with $L = 3$ sites, $t = 1$, $U/t = 22$ and 6 particles. Results were averaged among the three different sites of the unit cell.

From the discussed scenario, one may expect a metallic solution in the interval $1 < \mu/U < 2$, as it is well known that a metallic state is usually characterized by large density fluctuations. As visible in Figure 2, this is not the case, since the current is manifestly suppressed in this region of the parameters' space. The reason lies in the fact that metallicity occurs only when there are non-vanishing density fluctuations simultaneously in every lattice site. Therefore, it is instructive to look at the site-resolved distributions of local populations, shown in Figure 4 and to the site-resolved particle fluctuations

$$F(j) = \sum_{n=0}^{3} n^2 p_n(j) - \left(\sum_{n=0}^{3} n p_n(j) \right)^2, \tag{6}$$

which are shown in Figure 5. Remarkably, when $1 < \mu/U < 2$, there are large density fluctuations in the low-energy sites, since $p_2(j) \approx p_3(j) \approx 1/2$ at $j = 1, 3$; while, in the high-energy site, the fluctuations are suppressed, since the only non-vanishing probability is $p_1(2) \approx 1$. This means that, while tunneling processes between nearest-neighbor low-energy sites are possible, tunneling process between low-energy and high-energy sites are still forbidden, the particles cannot overcome the potential barrier and the system is an insulator. The metallicity condition is instead satisfied when $\mu/U \approx 1$ and $\mu/U \approx 2$, where density fluctuations are simultaneously high in every lattice site. We can thus introduce $\min_j \sqrt{F(j)}$, which represents the bottleneck of charge fluctuations along the chain. This quantity is shown in Figure 6 along with the corresponding current. The comparison between the two quantities reveals the mechanism underlying interaction-resilient metallicity.
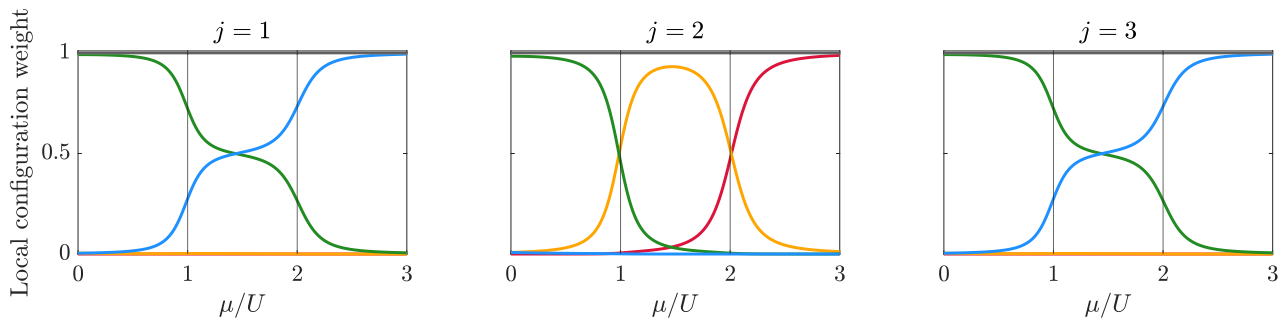

Figure 4. Site-resolved version of Figure 3. The same model parameters and the same color code were applied. The outer panels correspond to the two low-energy sites, while the central panel corresponds to the high-energy site.
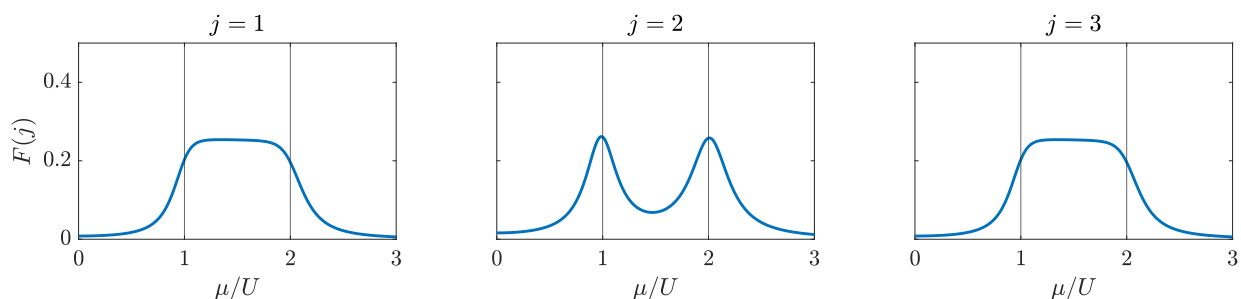

Figure 5. Site-resolved particle fluctuations (see Equation (6)). Same models parameters of Figures 3 and 4 were used. The outer panels correspond to the two low-energy sites, while the central panel corresponds to the high-energy site.
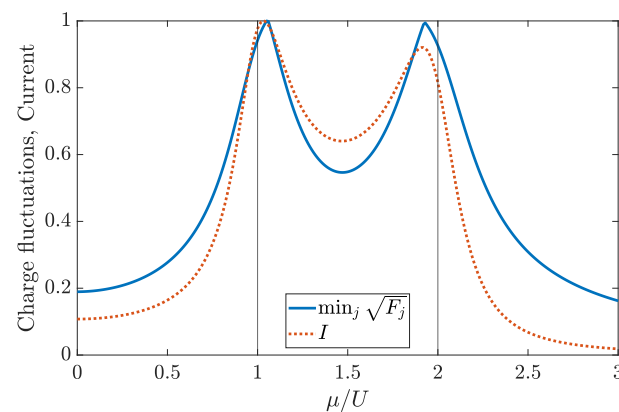
Figure 6. Comparison between the current flowing in the ring trimer (cut of Figure 2 at $U/t = 22$) and the minimum value of the site-resolved charge fluctuation (see Equation (6) and Figure 5). Both quantities were normalized to their maximum value (in the range $0 \leq \mu/U \leq 3$) for the sake of comparison.

4. Present and Future Perspectives

Mimicking the physics of Hund's metals [11] is just one of the many interesting possibilities offered by SU(N) atomic platforms. Tusi et al. [33] have recently demonstrated the possibility to realize flavor-selective Mott phases in three-flavor systems, whose intrinsic SU(3) symmetry is explicitly broken by Raman processes of the type $\Omega_{m,m'} \sum_i \left(c_{i,m}^\dagger c_{i,m'} + \text{h.c.} \right)$, which allow flavor redistribution between flavors m and m' to be obtained. In analogy with the well-known orbital-selective Mott phases [5–7], where terms breaking the inter-orbital symmetry (e.g., crystal-field splitting [4]) are known to determine the Mott localization of electrons in specific orbitals (hence the term "selective"), the authors of [33] showed that Raman processes which break the SU(3) symmetry of the parent Hamiltonian (1) constitute the seed of flavor-selective phenomena. More specifically, the authors experimentally realized the case $\Omega_{12} > 0$ and $\Omega_{23} = \Omega_{13} = 0$ and they observed that the combined effect of inter-flavor Raman coupling and interactions resulted in a phase where the two coupled flavors where less conductive than the uncoupled one. We remark that, both in the simulated solid-state models and in the simulating ultracold atomic platform, the symmetry-breaking term is just a *seed* for the emergence of orbital-selective or flavor-selective phases, which are, actually, fundamentally driven by interactions.

The possibility of realizing interaction-resilient metals with SU(3)-symmetric atoms and flavor-selective Mott phases with SU(3)-symmetry-broken atoms are just the first fruits of the rich harvest offered by suitably engineered ultracold atomic platforms. These results have shown that the path towards the quantum simulation of multicomponent materials is open and new spectacular results are expected concerning high-temperature superconductors [74] and interacting topological insulators [75], as well as magnetic crystals [76].

Abbreviations

The following abbreviations are used in this manuscript:

MI   Mott insulator
BI   Band insulator
SU (N)   Special unitary group of degree N

Appendix A. Hund's Metals in a Nutshell

In this Appendix, we briefly review the physics of Hund's metals in correlated materials, as described by the three-orbital Hubbard–Kanamori model. We refer to Refs. [9,11] and references therein for an exhaustive discussion. The Hubbard–Kanamori Hamiltonian reads

$$H = -\sum_{ij,ab,\sigma} t_{ij}^{ab} d_{ia\sigma}^\dagger d_{jb\sigma} + \sum_j H_{\text{int},j}, \tag{A1}$$

the local interaction term being

$$H_{\text{int},j} = U \sum_a n_{ja\uparrow} n_{ja\downarrow} + (U - 3J) \sum_{a<b,\sigma} n_{ja\sigma} n_{jb\sigma} + (U - 2J) \sum_{a\neq b} n_{ja\uparrow} n_{jb\downarrow}$$
$$+ J \sum_{a\neq b} d_{ja\uparrow}^\dagger d_{ja\downarrow}^\dagger d_{jb\downarrow} d_{jb\uparrow} - J \sum_{a\neq b} d_{ja\uparrow}^\dagger d_{ja\downarrow} d_{jb\downarrow}^\dagger d_{jb\uparrow}, \tag{A2}$$

where the operator $d_{ja\sigma}^\dagger$ creates an electron with spin $\sigma = \{\uparrow, \downarrow\}$ in the orbital $a = \{1, 2, 3\}$ of site j. The parameters $U > 0$ and $J > 0$ are, respectively, the standard Coulomb repulsion and Hund's exchange coupling; while t_{ij}^{ab} represents the hopping matrix element between site i orbital a and site j orbital b. In the strong coupling regime ($U \gg t_{ij}^{ab}$ and $J \gg t_{ij}^{ab}$) and for filling factor $\langle n \rangle = 2$, the physics of this model is ruled by the competition of two different correlated insulators; for $J/U \ll 1/3$, the ground state is a high-spin Mott-insulating state, while, for $J/U \gg 1/3$, it is a charge-disproportionated insulator, dubbed Hund's insulator (see Figure A1 for an illustrative representation). The former is stabilized by a strong Hubbard repulsion which penalizes inter-site charge fluctuations, while the latter is stabilized by Hund's exchange coupling, which favors high-spin and high-orbital-angular-momentum local configurations. In the atomic limit, these two insulators are degenerate, provided that $J/U = 1/3$. At this critical value, the system's ground state, as well as its low-energy excitations, undergoes a deep structural change, as schematically illustrated in Figure A2.
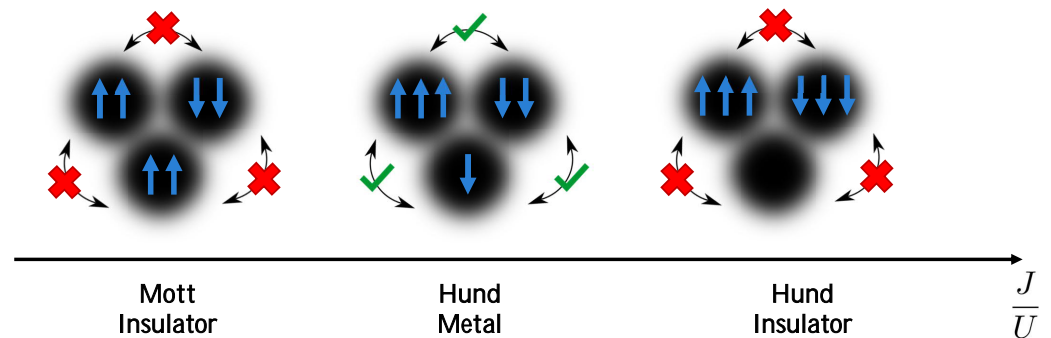

Figure A1. Pictorial representation of the three notable families of ground states of Hamiltonian (A1) for a three-site system with periodic boundary conditions and global filling $\langle n_j \rangle = 2$. The vertical blue arrows represent the z-component of the electronic spin. The green ticks (red crosses) are introduced to pictorially illustrate the (im)possible current flow in the ring trimer upon rotating it around its axis (see Section 3.2).
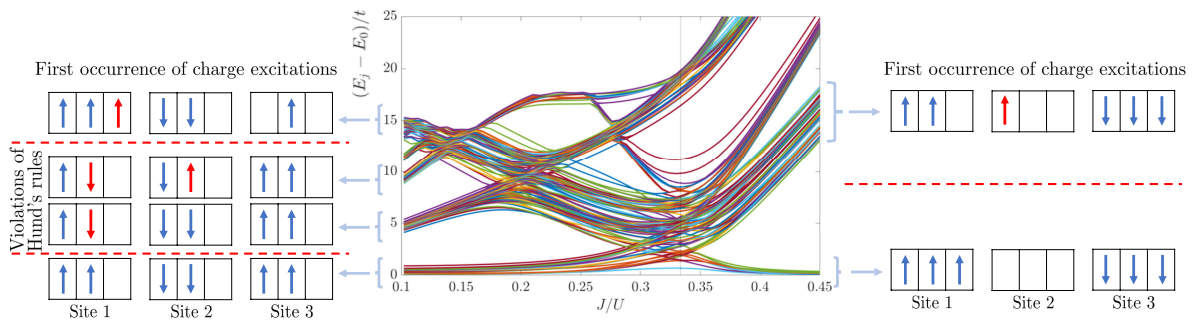
Figure A2. The first 3500 energy levels of Hamiltonian (A1) with $t_{ij}^{ab} = t\delta_{ab}\delta_{j,i\pm1}$, for $L = 3$ sites, 6 electrons, $t = 1$ and $U/t = 22$, as obtained from the exact numerical diagonalization (**central panel**). Each box is associated to an orbital and the vertical arrows represent the z-component of the electronic spin. For $J/U = 0.1$, the system's ground state is a high-spin Mott insulator and its excitations are essentially local violations of Hund's rules and, only at higher energy scales, inter-site charge fluctuations (**left panel**). For $J/U = 0.45$, the system's ground state is a Hund's insulator and its lowest-energy excitations are inter-site charge fluctuations (**right panel**). Interestingly, at $J/U = 1/3$, the discussed families of elementary excitations collapse, thus supporting the existence of an interaction-resilient metallic state, i.e., Hund's metal.

As discussed in Section 3.2, it is possible to probe the conduction properties of the ground state of Hamiltonian (A1) by means of the Peierls substitution (i.e., threading the ring with a magnetic flux), hence reconstructing a conductivity-based phase diagram by computing the expectation value of the current operator. As illustrated in Figure A3, the exact diagonalization of a minimal three-site cluster allows one to recognize the Mott-insulating, the Hund-insulating, as well as the Hund-metal state. These results, that we obtained in Ref. [11], confirm the ones [9] previously obtained within the dynamical mean-field theory [77], slave-spin mean-field theory [78] and rotation-invariant slave bosons [79]. The agreement among the presented results and the ones obtained with the aforementioned techniques is far from being trivial because completely different approximations are implied; thus, this leads to a cross-confirmation of the different approaches.
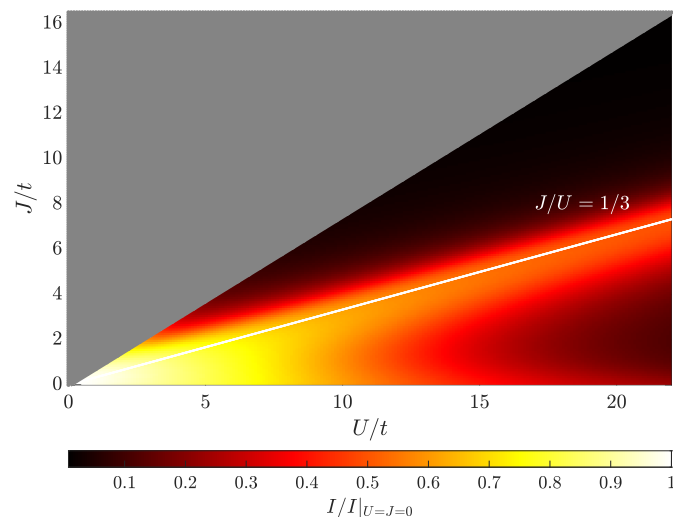

Figure A3. Expectation value of the current operator $I = \langle\psi_0| - \partial H/\partial\Phi|\psi_0\rangle$ as a function of U and J. The results were obtained by means of the exact numerical diagonalization of Hamiltonian (A1), with $t_{ij}^{ab} = t\delta_{ab}\delta_{j,i\pm1}$, in the case of a 3-site system, 6 particles, $t = 1$ and $\Phi = 0.1\pi$. One can appreciate a highly conductive stripe (centered about the line $J/U = 1/3$) separating two distinct insulating regions, Hund's metal. The grey-colored region is unphysical in the context of strongly correlated materials [9].

References

1. Haule, K.; Kotliar, G. Coherence–incoherence crossover in the normal state of iron oxypnictides and importance of Hund's rule coupling. *New J. Phys.* **2009**, *11*, 025021. [CrossRef]
2. de' Medici, L.; Mravlje, J.; Georges, A. Janus-Faced Influence of Hund's Rule Coupling in Strongly Correlated Materials. *Phys. Rev. Lett.* **2011**, *107*, 256401. [CrossRef]
3. de' Medici, L. Hund's coupling and its key role in tuning multiorbital correlations. *Phys. Rev. B* **2011**, *83*, 205112. [CrossRef]
4. de' Medici, L.; Hassan, S.R.; Capone, M.; Dai, X. Orbital-Selective Mott Transition out of Band Degeneracy Lifting. *Phys. Rev. Lett.* **2009**, *102*, 126401. [CrossRef]
5. Vojta, M. Orbital-selective Mott transitions: Heavy fermions and beyond. *J. Low Temp. Phys.* **2010**, *161*, 203–232. [CrossRef]
6. de'Medici, L.; Georges, A.; Biermann, S. Orbital-selective Mott transition in multiband systems: Slave-spin representation and dynamical mean-field theory. *Phys. Rev. B* **2005**, *72*, 205124. [CrossRef]
7. Ferrero, M.; Becca, F.; Fabrizio, M.; Capone, M. Dynamical behavior across the Mott transition of two bands with different bandwidths. *Phys. Rev. B* **2005**, *72*, 205126. [CrossRef]
8. Fanfarillo, L.; Valli, A.; Capone, M. Synergy between Hund-Driven Correlations and Boson-Mediated Superconductivity. *Phys. Rev. Lett.* **2020**, *125*, 177001. [CrossRef]
9. Isidori, A.; Berović, M.; Fanfarillo, L.; de' Medici, L.; Fabrizio, M.; Capone, M. Charge Disproportionation, Mixed Valence, and Janus Effect in Multiorbital Systems: A Tale of Two Insulators. *Phys. Rev. Lett.* **2019**, *122*, 186401. [CrossRef]
10. Chatzieleftheriou, M.; Berović, M.; Villar Arribi, P.; Capone, M.; de' Medici, L. Enhancement of charge instabilities in Hund's metals by breaking of rotational symmetry. *Phys. Rev. B* **2020**, *102*, 205127. [CrossRef]
11. Richaud, A.; Ferraretto, M.; Capone, M. Interaction-resistant metals in multicomponent Fermi systems. *Phys. Rev. B* **2021**, *103*, 205132. [CrossRef]
12. Stadler, K.M.; Kotliar, G.; Lee, S.S.B.; Weichselbaum, A.; von Delft, J. Differentiating Hund from Mott physics in a three-band Hubbard-Hund model: Temperature dependence of spectral, transport, and thermodynamic properties. *Phys. Rev. B* **2021**, *104*, 115107. [CrossRef]
13. de' Medici, L.; Hassan, S.R.; Capone, M. Genesis of Coexisting Itinerant and Localized Electrons in Iron Pnictides. *J. Supercond. Nov. Magn.* **2009**, *22*, 535–538. [CrossRef]
14. de' Medici, L.; Giovannetti, G.; Capone, M. Selective Mott Physics as a Key to Iron Superconductors. *Phys. Rev. Lett.* **2014**, *112*, 177001. [CrossRef]
15. Kugler, F.B.; Zingl, M.; Strand, H.U.R.; Lee, S.S.B.; von Delft, J.; Georges, A. Strongly Correlated Materials from a Numerical Renormalization Group Perspective: How the Fermi-Liquid State of Sr_2RuO_4 Emerges. *Phys. Rev. Lett.* **2020**, *124*, 016401. [CrossRef]
16. Merkel, M.E.; Ederer, C. Charge disproportionation and Hund's insulating behavior in a five-orbital Hubbard model applicable to d^4 perovskites. *Phys. Rev. B* **2021**, *104*, 165135. [CrossRef]
17. Zhang, X.; Bishof, M.; Bromley, S.L.; Kraus, C.V.; Safronova, M.S.; Zoller, P.; Rey, A.M.; Ye, J. Spectroscopic observation of SU(N)-symmetric interactions in Sr orbital magnetism. *Science* **2014**, *345*, 1467. [CrossRef]
18. Taie, S.; Yamazaki, R.; Sugawa, S.; Takahashi, Y. An SU(6) Mott insulator of an atomic Fermi gas realized by large-spin Pomeranchuk cooling. *Nat. Phys.* **2012**, *8*, 825. [CrossRef]
19. Ottenstein, T.B.; Lompe, T.; Kohnen, M.; Wenz, A.N.; Jochim, S. Collisional Stability of a Three-Component Degenerate Fermi Gas. *Phys. Rev. Lett.* **2008**, *101*, 203202. [CrossRef]
20. Huckans, J.H.; Williams, J.R.; Hazlett, E.L.; Stites, R.W.; O'Hara, K.M. Three-Body Recombination in a Three-State Fermi Gas with Widely Tunable Interactions. *Phys. Rev. Lett.* **2009**, *102*, 165302. [CrossRef]
21. Gorshkov, A.V.; Hermele, M.; Gurarie, V.; Xu, C.; Julienne, P.S.; Ye, J.; Zoller, P.; Demler, E.; Lukin, M.D.; Rey, A. Two-orbital SU(N) magnetism with ultracold alkaline-earth atoms. *Nat. Phys.* **2010**, *6*, 289. [CrossRef]
22. Cazalilla, M.A.; Ho, A.; Ueda, M. Ultracold gases of ytterbium: Ferromagnetism and Mott states in an SU(6) Fermi system. *New J. Phys.* **2009**, *11*, 103033. [CrossRef]
23. Pagano, G.; Mancini, M.; Cappellini, G.; Lombardi, P.; Schäfer, F.; Hu, H.; Liu, X.J.; Catani, J.; Sias, C.; Inguscio, M.; et al. A one-dimensional liquid of fermions with tunable spin. *Nat. Phys.* **2014**, *10*, 198. [CrossRef]
24. Zhang, R.; Cheng, Y.; Zhai, H.; Zhang, P. Orbital Feshbach resonance in alkali-earth atoms. *Phys. Rev. Lett.* **2015**, *115*, 135301. [CrossRef] [PubMed]
25. Pagano, G.; Mancini, M.; Cappellini, G.; Livi, L.; Sias, C.; Catani, J.; Inguscio, M.; Fallani, L. Strongly interacting gas of two-electron fermions at an orbital Feshbach resonance. *Phys. Rev. Lett.* **2015**, *115*, 265301. [CrossRef]
26. Höfer, M.; Riegger, L.; Scazza, F.; Hofrichter, C.; Fernandes, D.; Parish, M.; Levinsen, J.; Bloch, I.; Fölling, S. Observation of an orbital interaction-induced Feshbach resonance in Yb 173. *Phys. Rev. Lett.* **2015**, *115*, 265302. [CrossRef]
27. Cappellini, G.; Mancini, M.; Pagano, G.; Lombardi, P.; Livi, L.; de Cumis, M.S.; Cancio, P.; Pizzocaro, M.; Calonico, D.; Levi, F.; et al. Direct observation of coherent interorbital spin-exchange dynamics. *Phys. Rev. Lett.* **2014**, *113*, 120402. [CrossRef]
28. Scazza, F.; Hofrichter, C.; Höfer, M.; De Groot, P.; Bloch, I.; Fölling, S. Observation of two-orbital spin-exchange interactions with ultracold SU(N)-symmetric fermions. *Nat. Phys.* **2014**, *10*, 779. [CrossRef]
29. Del Re, L.; Capone, M. Selective insulators and anomalous responses in three-component fermionic gases with broken SU(3) symmetry. *Phys. Rev. A* **2018**, *98*, 063628. [CrossRef]

30. Cazalilla, M.A.; Rey, A.M. Ultracold Fermi gases with emergent SU(N) symmetry. *Rep. Prog. Phys.* **2014**, *77*, 124401. [CrossRef]
31. Mancini, M.; Pagano, G.; Cappellini, G.; Livi, L.; Rider, M.; Catani, J.; Sias, C.; Zoller, P.; Inguscio, M.; Dalmonte, M.; et al. Observation of chiral edge states with neutral fermions in synthetic Hall ribbons. *Science* **2015**, *349*, 1510–1513. [CrossRef] [PubMed]
32. A. Pérez-Romero, R. Franco, J.S.V. Phase diagram of the SU(3) Fermi–Hubbard model with next-neighbor interactions. *Eur. Phys. J. B* **2021**, *94*, 229. [CrossRef]
33. Tusi, D.; Franchi, L.; Livi, L.F.; Baumann, K.; Orenes, D.B.; Del Re, L.; Barfknecht, R.E.; Zhou, T.; Inguscio, M.; Cappellini, G.; et al. Flavour-selective localization in interacting lattice fermions via SU(N) symmetry breaking. *arXiv* **2021**, arXiv:2104.13338.
34. Messer, M.; Desbuquois, R.; Uehlinger, T.; Jotzu, G.; Huber, S.; Greif, D.; Esslinger, T. Exploring Competing Density Order in the Ionic Hubbard Model with Ultracold Fermions. *Phys. Rev. Lett.* **2015**, *115*, 115303. [CrossRef]
35. Sebby-Strabley, J.; Anderlini, M.; Jessen, P.S.; Porto, J.V. Lattice of double wells for manipulating pairs of cold atoms. *Phys. Rev. A* **2006**, *73*, 033605. [CrossRef]
36. Lahiri, S.; Mondal, S.; Singh, M.; Mishra, T. Mott insulator phases of nonlocally coupled bosons in bilayer optical superlattices. *Phys. Rev. A* **2020**, *101*, 063624. [CrossRef]
37. Becker, C.; Soltan-Panahi, P.; Kronjaeger, J.; Dörscher, S.; Bongs, K.; Sengstock, K. Ultracold quantum gases in triangular optical lattices. *New J. Phys.* **2010**, *12*, 065025. [CrossRef]
38. Jo, G.B.; Guzman, J.; Thomas, C.K.; Hosur, P.; Vishwanath, A.; Stamper-Kurn, D.M. Ultracold Atoms in a Tunable Optical Kagome Lattice. *Phys. Rev. Lett.* **2012**, *108*, 045305. [CrossRef]
39. Fabrizio, M.; Gogolin, A.O.; Nersesyan, A.A. From Band Insulator to Mott Insulator in One Dimension. *Phys. Rev. Lett.* **1999**, *83*, 2014–2017. [CrossRef]
40. Wilkens, T.; Martin, R.M. Quantum Monte Carlo study of the one-dimensional ionic Hubbard model. *Phys. Rev. B* **2001**, *63*, 235108. [CrossRef]
41. Kampf, A.P.; Sekania, M.; Japaridze, G.I.; Brune, P. Nature of the insulating phases in the half-filled ionic Hubbard model. *J. Phys. Condens. Matter* **2003**, *15*, 5895. [CrossRef]
42. Manmana, S.R.; Meden, V.; Noack, R.M.; Schönhammer, K. Quantum critical behavior of the one-dimensional ionic Hubbard model. *Phys. Rev. B* **2004**, *70*, 155115. [CrossRef]
43. Batista, C.D.; Aligia, A.A. Exact Bond Ordered Ground State for the Transition between the Band and the Mott Insulator. *Phys. Rev. Lett.* **2004**, *92*, 246405. [CrossRef] [PubMed]
44. Torio, M.E.; Aligia, A.A.; Japaridze, G.I.; Normand, B. Quantum phase diagram of the generalized ionic Hubbard model for AB$_n$ chains. *Phys. Rev. B* **2006**, *73*, 115109. [CrossRef]
45. Chattopadhyay, A.; Bag, S.; Krishnamurthy, H.R.; Garg, A. Phase diagram of the half-filled ionic Hubbard model in the limit of strong correlations. *Phys. Rev. B* **2019**, *99*, 155127. [CrossRef]
46. Garg, A.; Krishnamurthy, H.R.; Randeria, M. Can Correlations Drive a Band Insulator Metallic? *Phys. Rev. Lett.* **2006**, *97*, 046403. [CrossRef]
47. Paris, N.; Bouadim, K.; Hebert, F.; Batrouni, G.G.; Scalettar, R.T. Quantum Monte Carlo Study of an Interaction-Driven Band-Insulator–to–Metal Transition. *Phys. Rev. Lett.* **2007**, *98*, 046403. [CrossRef]
48. Bouadim, K.; Paris, N.; Hébert, F.; Batrouni, G.G.; Scalettar, R.T. Metallic phase in the two-dimensional ionic Hubbard model. *Phys. Rev. B* **2007**, *76*, 085112. [CrossRef]
49. Sengupta, P.; Sandvik, A.W.; Campbell, D.K. Bond-order-wave phase and quantum phase transitions in the one-dimensional extended Hubbard model. *Phys. Rev. B* **2002**, *65*, 155113. [CrossRef]
50. Sénéchal, D.; Perez, D.; Plouffe, D. Cluster perturbation theory for Hubbard models. *Phys. Rev. B* **2002**, *66*, 075129. [CrossRef]
51. Potthoff, M. Self-energy-functional approach: Analytical results and the Mott-Hubbard transition. *Eur. Phys. J. B-Condens. Matter Complex Syst.* **2003**, *36*, 335–348. [CrossRef]
52. Kotliar, G.; Savrasov, S.Y.; Pálsson, G.; Biroli, G. Cellular Dynamical Mean Field Approach to Strongly Correlated Systems. *Phys. Rev. Lett.* **2001**, *87*, 186401. [CrossRef]
53. Maier, T.; Jarrell, M.; Pruschke, T.; Hettler, M.H. Quantum cluster theories. *Rev. Mod. Phys.* **2005**, *77*, 1027–1080. [CrossRef]
54. Shiba, H.; Pincus, P.A. Thermodynamic Properties of the One-Dimensional Half-Filled-Band Hubbard Model. *Phys. Rev. B* **1972**, *5*, 1966–1980. [CrossRef]
55. Ullrich, C.A. (Spin-)density-functional theory for open-shell systems: Exact magnetization density functional for the half-filled Hubbard trimer. *Phys. Rev. A* **2019**, *100*, 012516. [CrossRef]
56. Schilling, C. Hubbard model: Pinning of occupation numbers and role of symmetries. *Phys. Rev. B* **2015**, *92*, 155149. [CrossRef]
57. Aligia, A.A. Effective Kondo Model for a Trimer on a Metallic Surface. *Phys. Rev. Lett.* **2006**, *96*, 096804. doi:10.1103/PhysRevLett.96.096804. [CrossRef]
58. Castro, E.; Foerster, A.; Santos, L. Interacting bosons in a triple well: Preface of many-body quantum chaos. *arXiv* **2021**, arXiv:2111.13714.
59. Richaud, A.; Penna, V. Pathway toward the formation of supermixed states in ultracold boson mixtures loaded in ring lattices. *Phys. Rev. A* **2019**, *100*, 013609. [CrossRef]
60. Penna, V.; Richaud, A. The phase-separation mechanism of a binary mixture in a ring trimer. *Sci. Rep.* **2018**, *8*, 10242. [CrossRef]

61. Richaud, A.; Zenesini, A.; Penna, V. The mixing-demixing phase diagram of ultracold heteronuclear mixtures in a ring trimer. *Sci. Rep.* **2019**, *9*, 6908. [CrossRef]
62. Richaud, A.; Penna, V. Phase separation can be stronger than chaos. *New J. Phys.* **2018**, *20*, 105008. [CrossRef]
63. Penna, V.; Richaud, A. Spatial Phase Separation of a Binary Mixture in a Ring Trimer. *J. Phys. Conf. Ser.* **2019**, *1206*, 012011. [CrossRef]
64. Richaud, A.; Penna, V. Quantum dynamics of bosons in a two-ring ladder: Dynamical algebra, vortexlike excitations, and currents. *Phys. Rev. A* **2017**, *96*, 013620. [CrossRef]
65. Penna, V.; Richaud, A. Two-species boson mixture on a ring: A group-theoretic approach to the quantum dynamics of low-energy excitations. *Phys. Rev. A* **2017**, *96*, 053631. [CrossRef]
66. Kohn, W. Theory of the Insulating State. *Phys. Rev.* **1964**, *133*, A171–A181. [CrossRef]
67. Fye, R.M.; Martins, M.J.; Scalapino, D.J.; Wagner, J.; Hanke, W. Drude weight, optical conductivity, and flux properties of one-dimensional Hubbard rings. *Phys. Rev. B* **1991**, *44*, 6909–6915. [CrossRef] [PubMed]
68. Giamarchi, T.; Shastry, B.S. Persistent currents in a one-dimensional ring for a disordered Hubbard model. *Phys. Rev. B* **1995**, *51*, 10915–10922. [CrossRef] [PubMed]
69. Scalapino, D.J.; White, S.R.; Zhang, S.C. Superfluid density and the Drude weight of the Hubbard model. *Phys. Rev. Lett.* **1992**, *68*, 2830–2833. [CrossRef] [PubMed]
70. Arwas, G.; Vardi, A.; Cohen, D. Superfluidity and Chaos in low dimensional circuits. *Sci. Rep.* **2015**, *5*, 13433. [CrossRef] [PubMed]
71. Chetcuti, W.J.; Polo, J.; Osterloh, A.; Castorina, P.; Amico, L. Probe for bound states of SU(3) fermions and colour deconfinement. *arXiv* **2021**, arXiv:2112.06950.
72. Morales-Molina, L.; Reyes, S.; Arévalo, E. Harnessing currents of particles for spectroscopy in small-ring lattices with binary mixtures. *Europhys. Lett.* **2020**, *131*, 36001. [CrossRef]
73. Chetcuti, W.J.; Haug, T.; Kwek, L.C.; Amico, L. Persistent Current of SU(N) Fermions. *SciPost Phys.* **2022**, *12*, 033. [CrossRef]
74. Lee, P.A.; Nagaosa, N.; Wen, X.G. Doping a Mott insulator: Physics of high-temperature superconductivity. *Rev. Mod. Phys.* **2006**, *78*, 17–85. [CrossRef]
75. Bernevig, B.A.; Hughes, T.L.; Zhang, S.C. Quantum spin Hall effect and topological phase transition in HgTe quantum wells. *Science* **2006**, *314*, 1757–1761. [CrossRef]
76. Barbarino, S.; Taddia, L.; Rossini, D.; Mazza, L.; Fazio, R. Magnetic crystals and helical liquids in alkaline-earth fermionic gases. *Nat. Commun.* **2015**, *6*, 8134. [CrossRef] [PubMed]
77. Georges, A.; Kotliar, G.; Krauth, W.; Rozenberg, M.J. Dynamical mean-field theory of strongly correlated fermion systems and the limit of infinite dimensions. *Rev. Mod. Phys.* **1996**, *68*, 13–125. [CrossRef]
78. de' Medici, L.; Capone, M. *The Iron Pnictide Superconductors: An Introduction and Overview*; Springer International: Cham, Germany, 2017; pp. 115–185.
79. Lechermann, F.; Georges, A.; Kotliar, G.; Parcollet, O. Rotationally invariant slave-boson formalism and momentum dependence of the quasiparticle weight. *Phys. Rev. B* **2007**, *76*, 155102. [CrossRef]